Intelligent nanoscope for rapid nanomaterial identification and classification

Journal:	*Lab on a Chip*
Manuscript ID	LC-ART-03-2022-000206.R1
Article Type:	Paper
Date Submitted by the Author:	23-May-2022
Complete List of Authors:	Jin, Geonsoo; Duke University, Mechanical Engineering and Materials Science
Hong, Seongwoo; Duke University, School of Medicine
Rich, Joseph; Duke University, Biomedical Engineering
Xia, Jianping; Duke University, Mechanical Engineering and Materials Science
Kim, Kyeri; Duke University, Department of Biomedical Engineering
You, Lingchong; Duke University, Department of Biomedical Engineering; Duke University, Center for Genomic and Computational Biology; Duke University, Department of Molecular Genetics and Microbiology
Zhao, Chenglong; University of Dayton, Physics; University of Dayton, Electro-Optics and Photonics
Huang, Tony; Duke University, Mechanical Engineering and Materials Science

SCHOLARONE™
Manuscripts

Lab on a Chip

Intelligent nanoscope for rapid nanomaterial identification and classification

Geonsoo Jin,[a] **Seongwoo Hong,**[b] **Joseph Rich,**[c] **Jianping Xia,**[a] **Kyeri Kim,**[c] **Lingchong You,**[cde] **Chenglong Zhao, ***[fg] **and Tony Jun Huang***[a]

Machine learning image recognition and classification of particles and materials is a rapidly expanding field. However, nanomaterial identification and classification are dependent on the image
10 resolution, the image field of view, and the processing time. Optical microscopes are one of the most widely utilized technologies in laboratories across the world, due to their nondestructive abilities to identify and classify critical micro-sized objects and processes, but identifying and classifying critical nano-sized objects and processes with a conventional microscope are outside of its capabilities, due to the diffraction limit of the optics and small field of view. To overcome these
15 challenges of nanomaterial identification and classification, we developed an intelligent nanoscope that combines machine learning and microsphere array-based imaging to: (1) surpass the diffraction limit of the microscope objective with microsphere imaging to provide high-resolution images; (2) provide large field-of-view imaging without the sacrifice of resolution by utilizing a microsphere array; and (3) rapidly classify nanomaterials using a deep convolution neural network. The
20 intelligent nanoscope delivers more than 46 magnified images from a single image frame so that we collected more than 1,000 images within 2 seconds. Moreover, the intelligent nanoscope achieves a 95% nanomaterial classification accuracy using 1,000 images of training sets, which is 45% more accurate than without the microsphere array. The intelligent nanoscope also achieves a 92% bacteria classification accuracy using 50,000 images of training sets, which is 35% more accurate than
25 without the microsphere array. This platform accomplished rapid, accurate detection and classification of nanomaterials with miniscule size differences. The capabilities of this device wield the potential to further detect and classify smaller biological nanomaterial, such as viruses or extracellular vesicles.

Introduction

30 Machine learning is a powerful tool for identifying and classifying material. One of the growing fields of machine learning applied to image recognition and classification is deep learning.[1-7] Deep learning is a part of the mathematically revolutionized machine learning algorithms which analyzes
35 information continuously with a given logic structure to draw similar conclusions as humans might. Within the field of deep learning, the convolutional neural network (CNN) is the most common tool for visual image analyzation and classification.[8-14] CNN exploits the spatial locality of an image by using
40 convolutional filters, and CNN image classification methods have demonstrated high accuracy while saving computational cost for size-based image classification, ranging from large objects (e.g., firearms) to small objects (e.g., nanomaterials).[15-22] However, image identification and classification of
45 nanomaterials is limited by the image resolution, the field of view of the sample, and the processing time.

Several inventions have been developed in order to assist in identifying and classifying smaller objects. For example, the invention of the optical microscope altered the course of history
50 for the identification of smaller material. Critical biological organisms and scientific processes have been analyzed and discovered through its use.[23-30] Recently, an electron
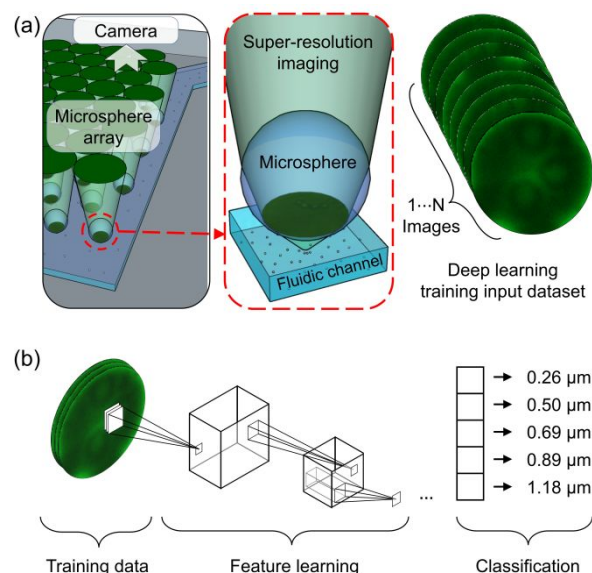
Fig. 1 (a) Schematic of the intelligent nanoscope setup, process, and data collection for deep learning training. The microsphere array and fluidic channel was fabricated to obtain deep learning training dataset images by super resolution imaging. (b) Schematic of the neural network process and nanoparticle classification. The gathered training datasets of each nanoparticle sample were used for feature learning by a convolutional neural network method. The trained model then classified the different sizes of nanoparticle samples.

microscopy assembled with nanofluidic coulter counting system was established for detection of drug-induced viruses.[31] Unlike some of the more advanced microscopy methods, the optical microscope is a universal instrument that is used in
5 many research and industrial areas, due to its nondestructive, inexpensive, and real-time imaging capabilities.[32, 33] Moreover, the rapid development of low-cost and high-frame-rate digital cameras makes fast sample identification and classification possible.[34-36] For example, recently a flow cytometric cell
10 sorting system with real-time intelligent image processor was developed to achieve high-throughput cell imaging and sorting.[37] Since the first generation of optical microscopes, the resolving power has significantly improved with the superior design of the objective lens. This high-resolution imaging has
15 been especially impactful in order to identify critical micro- and nano-sized particles, viruses, and bacteria that have been found to greatly impact humanity.[38-48] However, the identification and classification of nanomaterial targets through a conventional optical microscope has several limitations. For
20 example, the diffraction limit or resolution of a 20x objective lens is around 580 nm,[49] which makes it hard to resolve structures smaller than 580 nm. An objective lens with a higher NA can be used to increase the resolution but at the cost of a reduced field of view.

25 One particular method that has been employed to overcome the diffraction limit of a conventional optical microscope is by using optically transparent microspheres.[50-59] A microsphere focuses an incoming light to form a so-called photonic nanojet, which breaks the diffraction limit and essentially renders the
30 microsphere into a super-resolution imaging lens. Recently, a microsphere lens allowed for the successful detection of 50 nm gratings,[60] protein,[61] and plasmid DNA.[62, 63] Although the field of view of one microsphere is small, the field of view can be significantly increased by increasing the amount of
35 microspheres or scanning them in a controllable way.[64-68] This increase in the field of view increases the sample size of the images taken, thereby reducing sampling time. For example, single-nanomaterial detection with a microsphere array has recently been demonstrated.[69, 70]

40 By combining the innovations from the microsphere array optical imaging with CNN machine learning classification methods, we have developed the intelligent nanoscope. This platform can rapidly identify and classify nanomaterials with miniscule size differences. A large dataset of high-resolution
45 nanomaterial images can be quickly obtained from a microsphere array as training data for the CNN algorithm to rapidly distinguish and classify different sized nanomaterials. The intelligent nanoscope offers the following innovations: (1) simultaneous large field-of-view and super-resolution imaging
50 significantly reduces the sample data collection time and reveals additional training information for the CNN; (2) a deep CNN is applied to process the images and increase the accuracy for nanomaterial identification and classification. The intelligent nanoscope significantly reduces the number of
55 training data by 90 times and improves the training accuracy by two times compared to an optical microscope without the microsphere array. Moreover, we classified four different kinds of bacteria by using the intelligent nanoscope. Recently,

various research groups have reported bacteria classification
60 using optical microscopic images as training datasets for a CNN classification method.[71-73] These studies showed that target bacteria classification performance is dependent on its shape and size. By utilizing a microsphere array imaging method, we magnified the target sample image to acquire
65 detailed training datasets to enhance bacteria classification of bacteria of varying shapes and sizes. Some applications that can be used with this technology include bacteria type detection for infection diagnostic or nanoparticle size detection for nanomaterial synthesis feedback measurements. Overall, this
70 device achieves nondestructive, rapid, and accurate size-based classification of nanomaterials, showing great promise to extend to classifying smaller biological nanomaterials, such as extracellular vesicles or viruses, in the future.

Materials and methods

75 **Training data collection and deep neural network process**

Fig. 1 gives an overall depiction of the training image collection and deep neural network experiment process. The left panel of Fig. 1(a) shows a schematic of the intelligent nanoscope. The intelligent nanoscope consists of a microsphere array that can be placed on
80 the sample stage of a conventional optical microscope (20x, NA: 0.45, Eclipse LV100, Nikon, Japan). Magnified images were first captured through each barium titanate microsphere, as seen in the middle panel of Fig. 1(a), and then imaged on a camera through a low-magnification objective lens on the optical microscope.
85 Therefore, high-resolution images and a large field of view can be obtained simultaneously by incorporating the super-resolution capability of an array of microspheres.

Captured images were then categorized as training input datasets for deep learning (Fig. 1(a) right panel). To have
90 consistent image data acquisition, we imaged different sized SiO_2 nanoparticles (0.26 μm, 0.50 μm, 0.69 μm, 0.89 μm, 1.18 μm, Cospheric, USA) within the same microfluidic chip. SEM images and specification data of the properties of the nanoparticles are
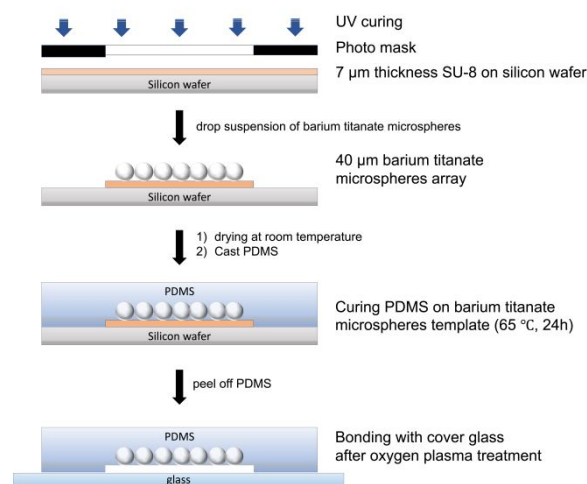
Fig. 2 Fabrication process of the microsphere array. 40 μm of barium titanite microspheres are immobilized with PDMS curing in a 7 μm tall microfluidic channel.
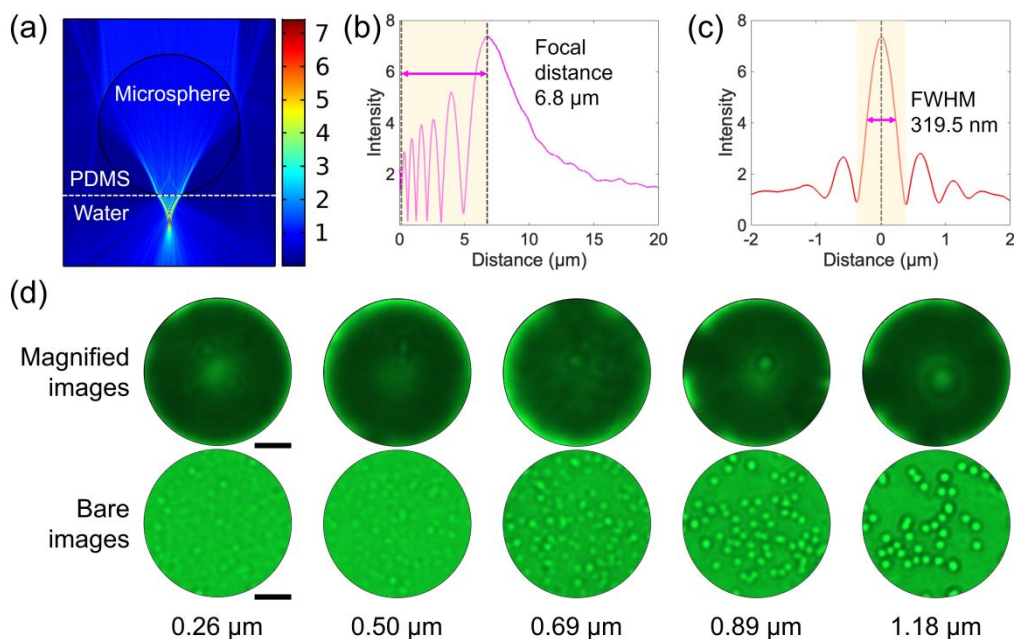
Fig. 3 (a) Finite element method simulation of electric field distribution around a barium titanite microsphere. Outer medium of microsphere is PDMS (n = 1.43), and the water (n =1.33) channel is beneath the PDMS and microsphere (n = 2.2). (b) Focal distance measurement from simulation results. (c) Full width half maximum of the photonic nanojets from 40 μm barium titanite microsphere simulation result. (d) Magnified images through a microsphere and bare nanoparticle images without a microsphere of the target SiO_2 nanoparticles. Scale bar is 5 μm.

shown in Supplementary Fig. 1. Between each experiment, the microfluidic channel was flushed with water and ethanol to ensure accurate training images. Furthermore, the microscope stage was also fixed to make sure all dataset's focal points were the same.

5 As shown in Fig. 1(b), we used a deep convolution neural network based on AlexNet to train and decompose class layers and then extract the distinctive features of each class.[74] The model architecture comprises of 5 convolution layers, 3 fully connected layers, and 3 × 3 max pooled, normalized, flattened, and dense 10 layers for reducing the overfitting with the rectified linear unit activation function. This model was then applied to separate known nanomaterial sizes to determine the model's accuracy for nanomaterial identification and classification.

Microsphere array fabrication

15 The microsphere array is fabricated by using standard soft-lithography procedures as depicted in Fig. 2.[75] First, a polydimethylsiloxane (PDMS) channel with a height of 7 μm is fabricated as follows: a photoresist (SU-8 10, MicroChem Inc., USA) was spin coated (4,000 RPM, 30 sec) on a 4-inch 20 polished single-sided silicon wafer (783, University Wafers, USA). After soft baking for 2 mins at 65 ℃ and 5 mins at 95 ℃, a carefully designed photomask was aligned to subsequently cure with UV for 10 seconds. Then, after post exposure baking (1 min at 65 ℃, 2 mins at 95 ℃), the uncured area was 25 developed by a SU-8 developer (Y020100 4000L1PE, Fisher Scientific, USA). In the following step, 40 μm sized barium titanite microspheres (refractive index: 2.2, Cospheric, USA) were mixed with DI water and dropped on the 3 mm^2 square channel in the fabricated mold. Next, after drying in room 30 temperature for 3 hours, mixed PDMS base and cross-linker in a 10:1 ratio (Sylgard 184, Dow Corning, USA) was applied

onto the barium titanite particle array mold and cured in a 65 ℃ oven for 24 hours. The cured PDMS channel was then peeled off from the wafer mold and punched at the inlet and outlet 35 connecting positions. Finally, the PDMS channel was bonded to an oxygen-plasma-treated 24 mm × 60 mm cover glass with no. 1 thickness (SuperSlips™ Micro Cover Glasses, VWR, USA) and incubated at 65℃ overnight.

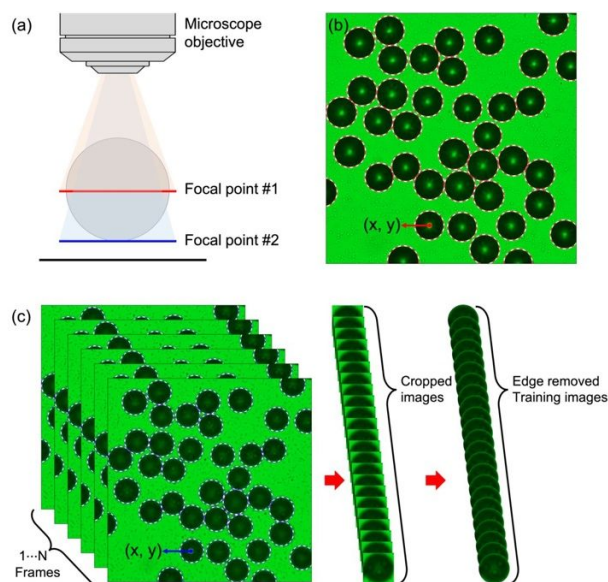40 **Experiment and microscope imaging setup**

The microsphere array is placed on the sample stage of an upright microscope (Eclipse LV100, Nikon, Japan) with a 20x objective lens (NA: 0.45, Nikon, Japan). A transmitted light source with a colored bandpass filter (FGV9 - Ø25 mm VG9, 45 Thorlabs, USA) was used to reduce chromatic aberration, and a 3.1 Mega pixels color CMOS camera (DFK 33UX265, Imagingsource, USA) was connected to the microscope. Particles of different sizes are injected to the microsphere array and imaged with the microsphere array on the microscope. The 50 sample nanomaterial was loaded and injected into the device by hand using a 1 ml syringe. As the flow reached a speed of approximately 15 to 20 μm/s in which the images would not be blurry at a 15 frames per second acquisition speed, the nanomaterial in the channel was captured using a CMOS 55 camera with a 20x objective lens.

Results and discussion

Finite element method simulation

A photonic nanojet is typically formed around a microsphere in a 60 homogenous medium. In order to validate that the PDMS and water boundaries did not significantly affect the formation of the

photonic nanojet, and in order to optimize the size and material of the microsphere and the microfluidic channel height, we performed a finite element method simulation, as seen in Fig. 3(a-c). To visualize the optical waves' propagation through the PDMS and 40 μm barium titanite microsphere, simulations were performed using the electromagnetic wave module in COMSOL Multiphysics software. The scattering boundary condition was applied on all the boundaries with an incident out-of-plane electric field amplitude of 1 V/m on the top. Fig. 3(a) shows the simulated electric field distribution around a barium titanite microsphere. The simulation result confirmed that the PDMS and water boundary did not significantly affect the formation of the photonic nanojet, as shown in Fig. 3(a). To determine the microfluidic channel height, we calculated a focal length of the microsphere, which is defined as the distance between the front surface of the microsphere and the center of the nanojet as shown in Fig. 3(b). The calculated focal distance was 6.8 μm, so we selected approximately 7 μm for the optimum channel height. In addition, to verify the image capability, we calculated the full width at half maximum (FWHM) of the photonic nanojets. The resulting FWHM of the photonic nanojet was 319.5 nm, indicating that the intelligent nanoscope could achieve around 115 nm ~ 201 nm of lateral resolution.[52] This is comparable to the 100x objective lens resolution. To compare with the resolution and the field of view size between intelligent nanoscope and conventional microscope, we added a quantitative table in the Supplementary Table S1.
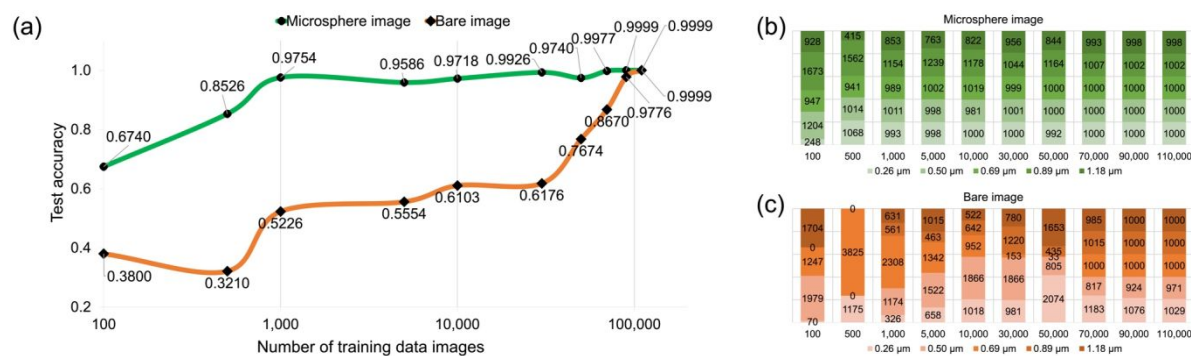
imaging for the machine learning training datasets. Nanomaterial images obtained through the microsphere array are shown in the first row of Fig. 3(d). Nanomaterial images in the absence of the microsphere arrays are shown in the second row of Fig. 3(d). The field of view was the same for both the microsphere and bare images for comparison. Due to the lack of microsphere magnification in the bare images, more nanomaterials are seen within the image. In this process, we maintained the same experimental conditions, including light intensity, imaging resolution, camera shutter speed, and field of view. The only changed condition was the change in focal point when collecting the bare images, in order to focus on the nanomaterials at the surface of the microfluidic channel. Images collected from these two conditions were used for the same deep learning training process. Each homogenous nanoparticle and bacteria samples were prepared in this work for reliable data collection. The nanomaterial concentration of the sample was selected to contain the greatest number of particles to form a single layer of nanomaterials in the field of view. This nanomaterial concentration was chosen in order to reduce the machine learning training dataset biases. These biases include the bias from an increase in empty space for the smaller sized nanomaterial, the bias from the increase in the probability of empty microspheres, and the bias from overlapping nanomaterial samples. Although the bias between empty space and the number of nanoparticles cannot be isolated, this concentration was applied to reduce the various biases of the system. This concentration was applied to both the microsphere imaging and bare imaging methods. By utilizing this nanomaterial concentration, a high classification performance is achieved for both imaging methods.

Deep learning training data preparation

Fig. 4 (a) Schematic of the two different focal points used through the microsphere. (b) Circle finding process from an image with focal point #1. Circle location information is stored. (c) The stored location is applied at image frames with focal point #2. Cropped image's edges are removed for making training data.

Image acquisition and comparison in different conditions

Although a microsphere could help to resolve and magnify the target sample, imaging the target sample without the microsphere array (bare imaging) needed to be considered in order to compare the machine learning performance with and without the increased resolution. Thus, we collected both microsphere imaging and bare
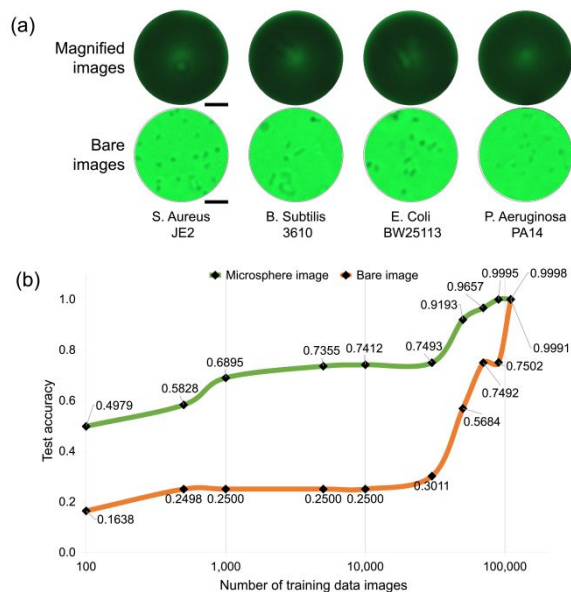
Fig. 5 (a) Nanoparticle classification accuracy for the different imaging methods with varying amounts of training data. 100 to 110,000 data images were used for the model training. (b), (c) Classification test results for each (b) microsphere image and (c) bare image of the five different sized particles for a given number of training images. 1,000 separately selected images from each category is inputted for the prediction test.

For images collected from the microsphere array, we collected images at two different focal planes as shown in Fig. 4(a). The image at focal plane #1 shows the image of the barium titanate microsphere that was utilized to locate the field of view of each
5 microsphere lens and provides accurate radius and center coordinates for image analysis. The focal plane #1 was fixed at the middle point of the barium titanate microsphere, which was around 20 μm from the microsphere's bottom, as depicted by the red line in Fig. 4(a). After taking a single image frame at
10 focal plane #1, the image focus was moved to focal plane #2, where the sample is located as shown in Fig. 4(a). At this focal plane, we could observe the magnified image through the microspheres, and the main data images were collected by a sequential image saving function from image capturing
15 software (IC capture – image acquisition, Imagingsource, USA) at 15 frames per second. We used a MATLAB circle finding function to obtain certain information such as the center coordinates and radius of each microsphere from an image at focal plane #1, as shown in Fig. 4(b). In total, 46 microspheres
20 were found from the image along with each microsphere's stored information. These 46 microspheres covered 51.16% of

the original field of view of the 20x objective lens. This allowed for a similar percentage of the field of view to compare both the microsphere and the bare imaging methods with the same
25 experimental conditions. Then, by applying the stored microsphere center coordinates and radius information, we could crop each magnified image belonging to the focal plane #2 dataset images, as seen in the left panel of Fig. 4(c). Since each cropped image had an unnecessary edge area which could
30 cause error for deep learning training, we removed the remaining edges and preserved the microsphere area from the cropped images, as shown in the right panel of Fig. 4(c).

Comparison between microsphere images and bare images

To verify the performance of nanomaterial classification, we
35 tested classification accuracy based on the size of the training datasets. Each category contained 1,000 images for each particle size, ranging from 0.26 μm to 1.18 μm. A range from 100 to 110,000 images were used for these training datasets. In each training procedure, we prepared 5,000 separate validation
40 data images and 1,000 prediction test images for each category of nanomaterials. Fig. 5(a) shows that the training model accuracy is dependent on the size of the training dataset. The imaging through the microsphere array has shown comparatively higher accuracy in categorization from a smaller dataset size. For
45 the case of a microsphere image, validation accuracy ranged from 67% to 97% with a corresponding training size of 100 to 1,000 images. This result indicates that datasets of 11 image frames can achieve higher than 85% classification capability, since a single image frame has 46 microsphere images as
50 training datasets. When the training dataset size is higher than 1,000 (*e.g.,* 22 image frames), the prediction test accuracy rises above 95%. In contrast, bare nanomaterial image without the microspheres showed that the prediction test accuracy could not exceed 95% until 90,000 images of training dataset sizes were
55 used. In order to achieve the same test accuracy of 97.5% from microsphere imaging, the bare imaging required 90 times more images for its training dataset. Fig. 5(b) and (c) show the classification results of the different sized particles for the two imaging nanomaterial methods for a given number of training data.

60 **Bacteria classification experiment**

Fig. 6 (a) Magnified images through a microsphere and bare microscopic images without a microsphere of the target bacteria samples with a 20x objective lens. Scale bar is 5 μm. (b) Bacteria classification accuracy for the different imaging methods with varying amounts of training data. 100 to 110,000 data images were used for the model training.

To demonstrate the capabilities of critical biological nanomaterial classification, we conducted a classification study of four different species of bacteria using the same experimental conditions. We used S. aureus JE2, B. subtilis 3610, E. coli BW25113, and P. aeruginosa PA14 in our experiments. A single colony was inoculated into 5 ml of Luria-Bertani (LB) broth medium in a test tube. Cultures were grown overnight (~17 hours) in a 37°C shaker shaking at 225 rpm. For imaging, the overnight culture was diluted 1:5 to the same medium and 1 µl of the diluted culture was loaded on the glass slide. Detailed bacteria images were taken under a Nikon Ti-E microscope with 100x objective lens (Supplementary Fig. 2). The average size difference from the microscope data for each bacteria type is in Supplemental Fig. S2e. Although the average size of each bacteria ranges from ~1 to 5 µm, the size difference between similarly shaped bacteria is on the nanoscale (<1 µm). Using the same protocols, we tested bacteria classification accuracy based on the size of the training datasets. We collected images through the microsphere array as shown in the first row of Fig. 6(a) to obtain each bacteria sample image for the machine learning training. Bacteria sample images in the absence of the microsphere arrays were also collected for comparison without the microsphere array imaging method, as shown in the second row of Fig. 6(a). A range from 100 to 110,000 images were used for the training datasets. 5,000 separate images of each bacteria sample were processed for test accuracy validation and 1,000 other separate images were prepared for prediction testing. Fig. 6(b) shows the training model accuracy for both the microsphere array imaging and the bare imaging methods. To achieve a test accuracy of ~92%, the bare imaging method took more than twice the amount of images for its training dataset. The classification results of the four different kinds of bacteria for the two imaging methods are shown in Supplementary Fig. 3. To test whether the present approach is distinguishing the bacterial cells by their shapes, we examined a bacteria classification accuracy for the different shaped bacteria subsets with varying amounts of training data in the supplementary figure S4. The results show that the different shaped samples require less training data, and that similarly shaped samples require 5 times larger data size to reach a 99% classification accuracy. A comparison between our bacteria classification technology and other bacteria classification technologies is provided in Supplemental Figure S2.

Conclusions

Here, we introduced the intelligent nanoscope imaging platform that utilizes a microsphere array to optically image and classify nanomaterials using a deep learning network. The microsphere array achieved a large field of view with high resolution for rapid data collection. By combining the microsphere array and machine learning, the intelligent nanoscope imaging platform achieved rapid classification of similarly sized particles. Greater than 95% nanomaterial classification test accuracy was achieved by 1,000 dataset images, which only took 2 seconds of collection time with a 15 frames/second camera. Also, nearly 92% bacteria classification test accuracy was achieved by 50,000 dataset images, which

only took ~73 seconds of collection time with a 15 frames/second camera. Given these features, this work could greatly assist in treating imperative biological nanomaterial threats, such as bacterial or viral infections, by rapidly and accurately classifying and identifying the biological nanomaterials. Future works of this technology include the classification of heterogenous samples and smaller bionanomaterial, including fluorescently tagged viral particles or small extracellular vesicles.

Conflict of Interests

Acknowledgements

a Thomas Lord Department of Mechanical Engineering and Materials Science, Duke University, Durham, NC 27708, USA.; E-mail: tony.huang@duke.edu
b Office of Biomedical Graduate Education, Duke University School of Medicine, Durham, NC 27710, USA.
c Department of Biomedical Engineering, Duke University, Durham, NC 27708, USA.; E-mail: you@duke.edu
d Center for Genomic and Computational Biology, Duke University, Durham, NC 27708, USA
e Department of Molecular Genetics and Microbiology, Duke University School of Medicine, Durham, NC 27708, USA
f Department of Physics, University of Dayton, 300 College Park, Dayton, Ohio 45469, USA.; E-mail: czhao1@udayton.edu
g Department of Electro-Optics and Photonics, University of Dayton, 300 College Park, Dayton, Ohio 45469, USA.

References:

1. T.-H. Chan, K. Jia, S. Gao, J. Lu, Z. Zeng and Y. Ma, *IEEE transactions on image processing*, 2015, **24**, 5017-5032.
2. K. He, X. Zhang, S. Ren and J. Sun, Proceedings of the IEEE conference on computer vision and pattern recognition, 2016.
3. C. Affonso, A. L. D. Rossi, F. H. A. Vieira and A. C. P. de Leon Ferreira, *Expert Systems with Applications*, 2017, **85**, 114-122.
4. L. Perez and J. Wang, *arXiv preprint arXiv:1712.04621*, 2017.
5. A. Mikołajczyk and M. Grochowski, 2018 international interdisciplinary PhD workshop (IIPhDW), 2018.
6. S. Li, W. Song, L. Fang, Y. Chen, P. Ghamisi and J. A. Benediktsson, *IEEE Transactions on Geoscience and Remote Sensing*, 2019, **57**, 6690-6709.
7. J. Zhang, Y. Xie, Q. Wu and Y. Xia, *Medical image analysis*, 2019, **54**, 10-19.
8. D. C. Ciresan, U. Meier, J. Masci, L. M. Gambardella and J. Schmidhuber, Twenty-second international joint conference on artificial intelligence, 2011.
9. A. G. Howard, *arXiv preprint arXiv:1312.5402*, 2013.

10. Q. Li, W. Cai, X. Wang, Y. Zhou, D. D. Feng and M. Chen, 2014 13th international conference on control automation robotics & vision (ICARCV), 2014.

11. S. Liu and W. Deng, 2015 3rd IAPR Asian conference on pattern recognition (ACPR), 2015.

12. T. Guo, J. Dong, H. Li and Y. Gao, 2017 IEEE 2nd International Conference on Big Data Analysis (ICBDA), 2017.

13. F. Sultana, A. Sufian and P. Dutta, 2018 Fourth International Conference on Research in Computational Intelligence and Communication Networks (ICRCICN), 2018.

14. S. S. Yadav and S. M. Jadhav, *Journal of Big Data*, 2019, **6**, 1-18.

15. G. Güven and A. B. Oktay, 2018 26th Signal Processing and Communications Applications Conference (SIU), 2018.

16. Y. Yamamoto, M. Hattori, J. Ohyama, A. Satsuma, N. Tanaka and S. Muto, *Microscopy*, 2018, **67**, 321-330.

17. M. Yayla, A. Toma, K.-H. Chen, J. E. Lenssen, V. Shpacovitch, R. Hergenröder, F. Weichert and J.-J. Chen, *Sensors*, 2019, **19**, 4138.

18. D. Kolenov, D. Davidse, J. Le Cam and S. Pereira, *Applied Optics*, 2020, **59**, 8426-8433.

19. A. Koyama, S. Miyauchi, K. i. Morooka, H. Hojo, H. Einaga and Y. Murakami, *Journal of Magnetism and Magnetic Materials*, 2021, **538**, 168225.

20. H. Jain, A. Vikram, A. Kashyap and A. Jain, 2020 International Conference on Electronics and Sustainable Communication Systems (ICESC), 2020.

21. G. K. Verma and A. Dhillon, Proceedings of the 7th International Conference on Computer and Communication Technology, 2017.

22. M. T. Bhatti, M. G. Khan, M. Aslam and M. J. Fiaz, *IEEE Access*, 2021, **9**, 34366-34382.

23. J. Hogg, *The Microscope: Its History, Construction, and Applications*, Illustrated London Libr., 1854.

24. J. Bennett, *Journal of Microscopy*, 1989, **155**, 267-280.

25. W. J. Croft, *Under the microscope: a brief history of microscopy*, World Scientific, 2006.

26. T. Araki, *Mechanical Engineering Reviews*, 2017, **4**, 16-00242-00216-00242.

27. T. Man, X. Zhu, Y. T. Chow, E. R. Dawson, X. Wen, A. N. Patananan, T. L. Liu, C. Zhao, C. Wu and J. S. Hong, *ACS nano*, 2019, **13**, 10835-10844.

28. N. Li, T. D. Canady, Q. Huang, X. Wang, G. A. Fried and B. T. Cunningham, *Nature communications*, 2021, **12**, 1-9.

29. Z. Wang, F. Li, J. Rufo, C. Chen, S. Yang, L. Li, J. Zhang, J. Cheng, Y. Kim and M. Wu, *The Journal of Molecular Diagnostics*, 2020, **22**, 50-59.

30. N. Hao, Z. Pei, P. Liu, H. Bachman, T. D. Naquin, P. Zhang, J. Zhang, L. Shen, S. Yang and K. Yang, *Small*, 2020, **16**, 2005179.

31. P. Kondylis, C. J. Schlicksup, N. E. Brunk, J. Zhou, A. Zlotnick and S. C. Jacobson, *Journal of the American Chemical Society*, 2018, **141**, 1251-1260.

32. A. Dixon, S. Damaskinos and M. Atkinson, *Nature*, 1991, **351**, 551.

33. E. Betzig and J. K. Trautman, *Science*, 1992, **257**, 189-195.

34. E. R. Fossum, *IEEE transactions on electron devices*, 1997, **44**, 1689-1698.

35. M. Bigas, E. Cabruja, J. Forest and J. Salvi, *Microelectronics journal*, 2006, **37**, 433-451.

36. S. A. Taylor, *UK: Xerox Research Centre Europe*, 1998.

37. A. Isozaki, H. Mikami, H. Tezuka, H. Matsumura, K. Huang, M. Akamine, K. Hiramatsu, T. Iino, T. Ito and H. Karakawa, *Lab on a Chip*, 2020, **20**, 2263-2273.

38. D. L. Farkas, *Nature biotechnology*, 2003, **21**, 1269-1271.

39. H. G. Abdelhady, S. Allen, S. J. Ebbens, C. Madden, N. Patel, C. J. Roberts and J. Zhang, *Nanotechnology*, 2005, **16**, 966.

40. M. Gruhlke and H. Rothe, *Combining coordinate measurement and nanometrology for large-range nanoscale metrology*, SPIE, 2007.

41. A. Imtiaz, T. M. Wallis and P. Kabos, *IEEE Microwave Magazine*, 2014, **15**, 52-64.

42. T. D. Canady, N. Li, L. D. Smith, Y. Lu, M. Kohli, A. M. Smith and B. T. Cunningham, *Proceedings of the National Academy of Sciences*, 2019, **116**, 19362-19367.

43. A. Ray, M. A. Khalid, A. Demčenko, M. Daloglu, D. Tseng, J. Reboud, J. M. Cooper and A. Ozcan, *Nature Communications*, 2020, **11**, 1-10.

44. P. B. Lillehoj, C. W. Kaplan, J. He, W. Shi and C.-M. Ho, *Journal of laboratory automation*, 2014, **19**, 42-49.

45. H. Shen, L. Chen, L. Ferrari, M.-H. Lin, N. A. Mortensen, S. Gwo and Z. Liu, *Nano letters*, 2017, **17**, 2234-2239.

46. M. Mancuso, L. Jiang, E. Cesarman and D. Erickson, *Nanoscale*, 2013, **5**, 1678-1686.

47. P. Chaturvedi, K. H. Hsu, A. Kumar, K. H. Fung, J. C. Mabon and N. X. Fang, *ACS nano*, 2009, **3**, 2965-2974.

48. Y. Gu, C. Chen, Z. Mao, H. Bachman, R. Becker, J. Rufo, Z. Wang, P. Zhang, J. Mai and S. Yang, *Science advances*, 2021, **7**, eabc0467.

49. R. Heintzmann and G. Ficz, *Briefings in Functional Genomics*, 2006, **5**, 289-301.

50. Z. Wang, N. Joseph, L. Li and B. Luk'Yanchuk, *Proceedings of the Institution of Mechanical Engineers, Part C: Journal of Mechanical Engineering Science*, 2010, **224**, 1113-1127.

51. H. Yang, N. Moullan, J. Auwerx and M. A. Gijs, *Small*, 2014, **10**, 1712-1718.

52. H. Yang, R. Trouillon, G. Huszka and M. A. Gijs, *Nano letters*, 2016, **16**, 4862-4870.

53. A. Bezryadina, J. Li, J. Zhao, A. Kothambawala, J. Ponsetto, E. Huang, J. Wang and Z. Liu, *Nanoscale*, 2017, **9**, 14907-14912.

54. A. Darafsheh, *Optics Letters*, 2017, **42**, 735-738.

55. C.-W. Chang, P.-Y. Li, Y. Tsao and S.-W. Chu, Plasmonics: Design, Materials, Fabrication, Characterization, and Applications XVI, 2018.

56. S. Yang, Y. Cao, Q. Shi, X. Wang, T. Chen, J. Wang and Y.-H. Ye, *The Journal of Physical Chemistry C*, 2019, **123**, 28353-28358.

57. T. Zhang, P. Li, H. Yu, F. Wang, X. Wang, T. Yang, W. Yang, W. J. Li, Y. Wang and L. Liu, *Applied Surface Science*, 2020, **504**, 144375.

58. S. Lee, L. Li and Z. Wang, *Journal of Optics*, 2013, **16**, 015704.

59. L. Chen, Y. Zhou, R. Zhou and M. Hong, *Iscience*, 2020, **23**, 101211.

60. Z. Wang, W. Guo, L. Li, B. Luk'yanchuk, A. Khan, Z. Liu, Z. Chen and M. Hong, *Nature communications*, 2011, **2**, 218.

61. A. Brettin, K. F. Blanchette, Y. Nesmelov, N. I. Limberopoulos, A. M. Urbas and V. N. Astratov, 2016 IEEE National Aerospace and Electronics Conference (NAECON) and Ohio Innovation Summit (OIS), 2016.

62. Y.-C. Li, H.-B. Xin, H.-X. Lei, L.-L. Liu, Y.-Z. Li, Y. Zhang and B.-J. Li, *Light: Science & Applications*, 2016, **5**, e16176.

63. Y. Li, H. Xin, X. Liu, Y. Zhang, H. Lei and B. Li, *ACS nano*, 2016, **10**, 5800-5808.

64. G. Jin, H. Bachman, T. D. Naquin, J. Rufo, S. Hou, Z. Tian, C. Zhao and T. J. Huang, *ACS nano*, 2020, **14**, 8624-8633.

65. J. Rufo, F. Cai, J. Friend, M. Wiklund and T. J. Huang, *Nature Reviews Methods Primers*, 2022, **2**, 30.

66. S. Yang, Z. Tian, Z. Wang, J. Rufo, P. Li, J. Mai, J. Xia, H. Bachman, P.-H. Huang and M. Wu, *Nature Materials*, 2022, **21**, 540-546.

67. P. Zhang, H. Bachman, A. Ozcelik and T. J. Huang, *Annual Review of Analytical Chemistry*, 2020, **13**, 17-43.

68. P. Liu, Z. Tian, K. Yang, T. D. Naquin, N. Hao, H. Huang, J. Chen, Q. Ma, H. Bachman and P. Zhang, *Science Advances*, 2022, **8**, eabm2592.

69. H. Yang, M. Cornaglia and M. A. Gijs, *Nano letters*, 2015, **15**, 1730-1735.

70. P. Ghenuche, J. de Torres, P. Ferrand and J. Wenger, *Applied Physics Letters*, 2014, **105**, 131102.

71. T. Mhathesh, J. Andrew, K. Martin Sagayam and L. Henesey, in *Intelligence in Big Data Technologies—Beyond the Hype*, Springer, 2021, pp. 419-431.

72. D. Połap and M. Woźniak, 2019 International Joint Conference on Neural Networks (IJCNN), 2019.

73.   M. F. Wahid, T. Ahmed and M. A. Habib, 2018 10th
       international conference on electrical and computer engineering
       (ICECE), 2018.
74.   A. Krizhevsky, I. Sutskever and G. E. Hinton, *Advances in
       neural information processing systems*, 2012, **25**.
75.   Y. Xia and G. M. Whitesides, *Annual review of materials
       science*, 1998, **28**, 153-184.

5